EUROPEAN ORGANIZATION FOR NUCLEAR RESEARCH

CERN–PPE/96–58
21 March 1996

OBSERVABLES IN HIGH-STATISTICS MEASUREMENTS OF THE REACTION $\bar{p}p \to \bar{\Lambda}\Lambda$

P.D. Barnes[1)], P. Birien[2)], W. Breunlich[3)], R. Bröders[4)], H. Dennert[6)], G. Diebold[1)], W. Dutty[2)], R.A. Eisenstein[5)], W. Eyrich[6)], H. Fischer[2)], R. von Frankenberg[4)], G. Franklin[1)], J. Franz[2)], R. Geyer[6)], N. Hamann[†7)], J. Hauffe[6)], D. Hertzog[5)], A. Hofmann[†6)], T. Johansson[8)], K. Kilian[4)], M. Kirsch[6)], R.A. Kraft[6)], N. Nägele[3)], W. Oelert[4)], S. Ohlsson[8)], B. Quinn[1)], K. Röhrich[4)], E. Rössle[2)], K. Sachs[4)], H. Schledermann[2)], H. Schmitt[2)], R. Schumacher[1)], T. Sefzick[4)], G. Sehl[4)], J. Seydoux[1)], F. Stinzing[6)], R. Tayloe[5)], R. Todenhagen[2)], V. Zeps[1)], M. Ziolkowski[4)]

Abstract

Associated strangeness production was studied in the $\bar{p}p \to \bar{\Lambda}\Lambda \to \bar{p}\pi^+p\pi^-$ reaction at the CERN antiproton facility LEAR using the experimental set-up of PS185. Results from two high–statistics measurements at incident antiproton momenta of 1.642 and 1.918 GeV/c are reported. Approximately 40 000 reconstructed events at each momentum have allowed us to measure the total and differential cross-sections, the spin polarizations, the spin correlations, and the singlet fractions of the $\Lambda\bar{\Lambda}$ pair. Since the decays of both the Λ and the $\bar{\Lambda}$ were simultaneously observed in the same detector, we are able to provide upper limits on CP and CPT violation phenomena in the weak interaction.

(Submitted to Physical Review C)

[1)] Carnegie-Mellon University, Pittsburgh, Pennsylvania 15260, USA.
[2)] Universität Freiburg, Freiburg, Germany.
[3)] Institut für Mittelenergiephysik der ÖAW, Vienna, Austria.
[4)] Institut für Kernphysik der KFA Jülich, Jülich, Germany.
[5)] University of Illinois, Urbana, Illinois 61801, USA.
[6)] Universität Erlangen-Nürnberg, Nürnberg, Germany.
[7)] CERN, Geneva, Switzerland.
[8)] Uppsala University, Uppsala, Sweden.
[†] Deceased

1 Introduction

In a systematic study over several years [1]–[26], the PS185 Collaboration at the Low-Energy Antiproton Ring (LEAR) at CERN has been investigating antihyperon–hyperon ($\bar{Y}Y$) production and decay via the reaction $\bar{p}p \to \bar{Y}Y$. The focus of this work is to explore the physics of strange-quark production and the role of the s quark in the configuration of the emerging hyperons. Our experiments build on several earlier studies [27]–[31] which used incident momenta ranging from 1.5 to 6 GeV/c. The principal advantages of the recent PS185 studies lie in their momentum resolution and consequent ability to approach very close to the reaction threshold, their generally high statistics, and the measurement of an almost complete set of spin observables. The high quality of the resulting data set is due in large measure to the extraordinary qualities of the LEAR/CERN accelerator complex.

Our studies, involving production of the Λ and Σ hyperons, have taken place at several incident momenta, ranging from the threshold for $\bar{\Lambda}\Lambda$ production (1.4356 GeV/c), to momenta close to the upper limit of the LEAR facility (2.0 GeV/c). For $\bar{\Lambda}\Lambda$ production, the latter value corresponds to an excess kinetic energy ($\epsilon = \sqrt{s} - m_{\bar{\Lambda}} - m_{\Lambda}$) of 199 MeV. We have measured precise values for the total and differential cross-sections at each incident momentum. In most cases (excepting those closest to threshold) we have also been able to measure the spin polarizations and correlations of the outgoing hyperons. It is hoped that this additional information about the basic amplitudes will be of significant help in constraining theoretical models of strange-quark production.

At each momentum studied, the crucial role played by strong annihilation in $\bar{p}p$ reactions is readily apparent. Indeed, the reaction cross-sections for the two-body hyperon final states are very small compared to those for annihilation into pionic final states. For example, the total cross-section for $\bar{\Lambda}\Lambda$ production is observed to rise steeply from threshold to excess energies around 50 MeV ($p_{\bar{p}} \sim 1.6$ GeV/c) as phase space increases, followed by a slow increase from 60 μb to about 100 μb at 2 GeV/c. This value is about 1000 times smaller than that observed for pion production. Similarly, our measured differential cross-sections and polarizations [1]–[24] display features that are characteristic of strong-interaction dynamics [32], [33]. These matters are discussed further below.

In the lower momentum range, PS185 data very close to threshold have been published [22], [24]. Data taking has recently been extended in this region to explore an unexpected structure in the total cross-section behaviour at $\epsilon \sim 1$ MeV excitation energy [24]. In the intermediate and upper momentum ranges, additional data are currently being analysed [1], [2], [12], [18].

The reaction dynamics of the $\bar{p}p \to \bar{\Lambda}\Lambda$ transition have been studied in many theoretical papers [34]–[61]. These descriptions have been of three general types:

- the strangeness production originates from the t-channel exchange of K mesons [34]–[40];
- the process originates from the s-channel annihilation of a $\bar{u}u$ pair and the subsequent production of an $\bar{s}s$ pair that is accompanied by four 'spectator' quarks [41]–[51] (other work has focused on quark descriptions via quark counting rules [52]);
- model-independent analyses of the low-momentum data, which are based on a partial-wave amplitude decomposition [53]–[55]. Since only a few partial waves contribute here, it may be possible to learn more about the underlying reaction mechanism.

Additional work [56]–[58] has also been done in the threshold region to study the possible anomaly [24] in the total cross-section data mentioned above.

The typical collision distances are expected to be short due to the large momentum transfer necessary to create the final-state hyperons. This leads to the expectation that quark effects might be important, even though K meson exchanges describe the experimental data very well. However, given the strongly-absorbing nature of these reactions, we expect that initial- and final-state interactions will be of major significance, and may hinder a deeper understanding of absorptive processes, clouding our ability to learn more about the detailed nature of the production process. In order to deal with a mixture of strongly- and weakly-coupled channels acting within this same problem, coupled-channels techniques [59]–[61] have been used to interpret the data.

In this paper we present two high-statistics measurements of the $\bar{p}p \to \bar{\Lambda}\Lambda \to \bar{p}\pi^+p\pi^-$ process. The data set at 1.642 GeV/c incident $\bar{p}$ momentum lies just below the opening of the $\bar{p}p \to \bar{\Lambda}\Sigma^0 + \text{c.c.}$ channel. The other set, taken at 1.918 GeV/c, lies above the thresholds for the $\bar{p}p \to \bar{\Sigma}^{\pm}\Sigma^{\pm}$ channels. Measured values for the $\bar{\Lambda}\Sigma^0 + \text{c.c.}$ [18] and $\bar{\Sigma}^{\pm}\Sigma^{\pm}$ [6] cross-sections at these momenta will be presented in a forthcoming publication. They will augment the earlier $\bar{\Lambda}\Sigma^0 + \text{c.c.}$ data [25] published by PS185.

2 Detection and data analysis

2.1 Detector

The PS185 experiment is designed for high-acceptance measurements of the $\bar{p}p \to \bar{\Lambda}\Lambda$ reaction from very near threshold to 2 GeV/c over the entire 4π solid angle. The charged weak-decay mode $\bar{p}p \to \bar{\Lambda}\Lambda \to \bar{p}\pi^+p\pi^-$ provides the signature that is used to determine events by kinematic fitting. It also permits a statistical determination of the final-state spin observables [62]. The experimental set-up, shown in Fig. 1, is described in detail in [1]–[23]. It is designed around a non-magnetic decay spectrometer consisting of a segmented-target neutral trigger system, a set of MWPC and MWDC tracking detectors, a fast scintillation detector (trigger) hodoscope, and a 'baryon identifier'. The latter consists of a 0.09 T magnetic solenoid, incorporating three drift chamber planes which are used to distinguish hyperon from antihyperon vertices.

For the data reported here, the target consisted of several small individual CH_2 elements, each having a diameter of 2.5 mm and a length of 2.5 mm. Three or four target elements were used, depending on the conditions desired for the run in question. Each target element was 'sandwiched' between and surrounded by an array of small scintillators in order to provide precise information about the incident momentum and the position of the reaction point, as well as a signature for the neutral-particle final state. A pure ^{12}C target cell allowed study of background events arising from carbon in the CH_2 target.

2.2 Data analysis

The analysis is based on reconstructing events with two Vs from the delayed decays of a $\bar{\Lambda}\Lambda$ pair. The decays lead to the charged particle pairs $\bar{p}\pi^+$ and $p\pi^-$. Two-dimensional tracks are fitted to hits in the MWPC and MWDC planes and then matched to form three-dimensional tracks. Candidate Vs are constructed from two three-dimensional tracks which intersect at a point downstream from the target and which are sufficiently coplanar with the interaction point. Candidate two-V events are formed if there are two Vs with vertices consistent with two-body kinematics. A full kinematic fit is performed to determine if the data agree with the $\bar{p}p \to \bar{\Lambda}\Lambda \to \bar{p}\pi^+p\pi^-$ hypothesis. Each V is assigned to a Λ or a $\bar{\Lambda}$ based on the sagitta of the decay tracks in the magnetic field of the

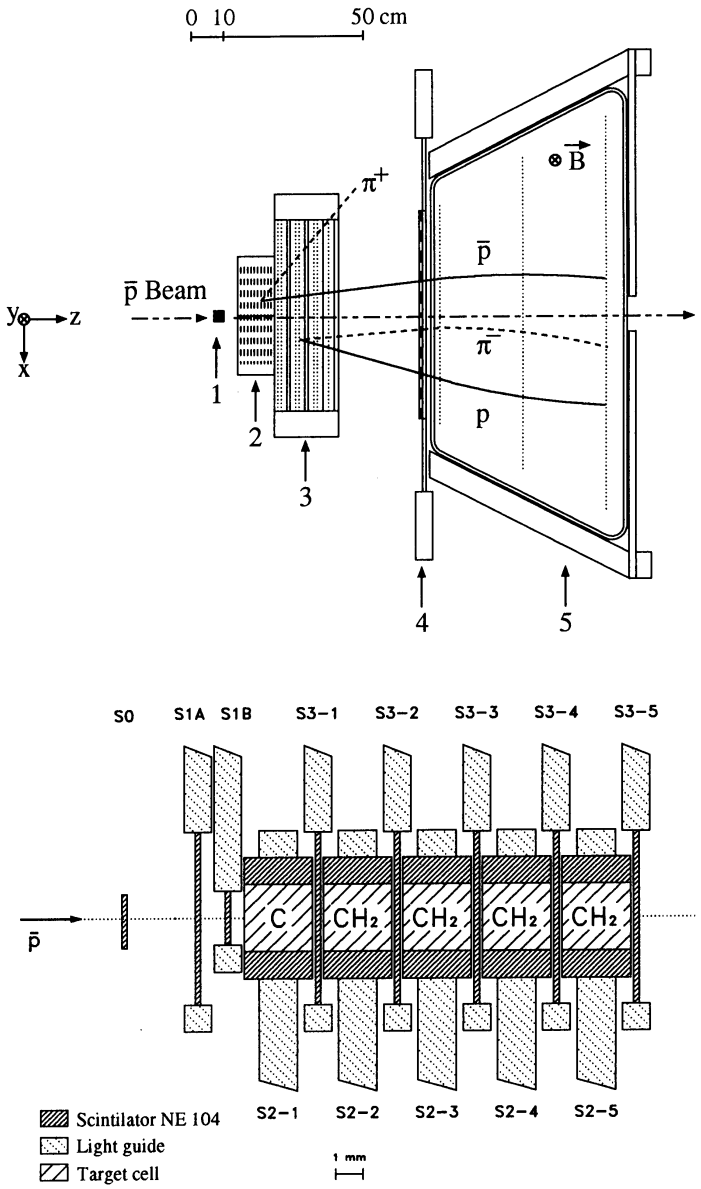

Figure 1: Overview of the PS185 detector system: (1) segmented neutral trigger target; (2) multiwire proportional chambers (MWPCs); (3) multiwire drift chambers (MWDCs); (4) scintillator hodoscope; (5) solenoid 'baryon identifier' with drift chambers. The lower part of the figure shows a detail of the segmented target.

'baryon identifier'. Since this situation is kinematically overconstrained, it is possible to obtain a $\Lambda\bar{\Lambda}$ sample which is almost free of background.

3 Evaluation of the cross-section

In order to evaluate the total and differential cross-sections, several corrections had to be performed on the data; these are outlined below. Fuller accounts can be found in [1]–[26].

- Since each $\bar{\mathrm{p}}$ in the beam was registered individually, a correction was made for approximately 0.7% loss of beam flux in each target cell due to nuclear interactions other than the channel of interest, and for straggling. In addition, the knockout of δ-electrons caused a trigger inefficiency requiring a correction of approximately 5% for a CH_2 cell and 2% for a ^{12}C cell.
- A correction due to $\bar{\mathrm{p}}\mathrm{p} \to \bar{\Lambda}\Lambda$ reactions from protons bound in the ^{12}C of the CH_2 cells was determined by reconstructing events from the special carbon cell installed for this purpose. This background was of the order of 5–10% and was subtracted.
- Corrections due to uncertainties in track fitting were addressed using a χ^2 criterion. The kinematic fitting procedure used generally required that $\chi^2 \leq 5$. Since this value is somewhat arbitrary, a Monte Carlo simulation was used to determine an appropriate correction factor, which was of the order of 5%.
- Corrections due to possible reactions of the decay particles in the detector material were made using known reaction cross-sections and detector density distributions, resulting in a correction of about 1.6%.
- Corrections due to the experimental acceptance, which ranges from 29% to 56% depending on the angle, included effects from online triggering, reconstruction efficiency, and baryon number identification. These were calculated by Monte Carlo models.
- Finally, the branching ratio for charged particle decay of the $\bar{\Lambda}\Lambda$ pair was taken into account by using the factor $(0.641 \pm 0.005)^2$ [63].

4 Spin observables

Spin observables are a crucial part of the physics we want to study in the $\bar{\mathrm{p}}\mathrm{p} \to \bar{\Lambda}\Lambda$ reaction. The density matrix formalism in the helicity basis ([33], [35], [64]) is a particularly clear and elegant way to follow the development of the spin states as the reaction progresses.

It is well known that the density matrix ρ, for a collection of *uncorrelated* spin-1/2 particles, can be written as $\rho = 1/2 \cdot (I + \vec{\sigma} \cdot \vec{P})$, where I is the 2×2 unit matrix, $\vec{\sigma}$ are the Pauli spin matrices, and $\vec{P}$ is the average spin polarization vector of the sample. Because the initial antiproton beam and the hydrogen target both consist of spin-1/2 particles which are assumed to be uncorrelated, the spins in the initial $\bar{\mathrm{p}}\mathrm{p}$ system can be represented by the following outer product of 2×2 density matrices:

$$\rho_{\bar{\mathrm{p}}\mathrm{p}} = \frac{1}{2}(I + \vec{\sigma} \cdot \vec{P})_{\bar{\mathrm{p}}} \otimes \frac{1}{2}(I + \vec{\sigma} \cdot \vec{P})_{\mathrm{p}} \ . \tag{1}$$

So, by construction, $\rho_{\bar{\mathrm{p}}\mathrm{p}}$ is a separable 4×4 matrix in $\bar{\mathrm{p}}\mathrm{p}$ spin space. When the initial polarizations are zero, the $\bar{\mathrm{p}}\mathrm{p}$ density matrix is $1/4 \cdot I$, where I is the unit matrix in 4×4 space.

To obtain the final-state density matrix $\rho_{\bar{\Lambda}\Lambda}$ from $\rho_{\bar{\mathrm{p}}\mathrm{p}}$, we operate with the strong interaction transition matrix T as follows:

$$\rho_{\bar{\Lambda}\Lambda} = T(\theta_{\bar{\Lambda}})\, \rho_{\bar{\mathrm{p}}\mathrm{p}}\, T^{\dagger}(\theta_{\bar{\Lambda}}) \ , \tag{2}$$

where θ is the scattering angle in the centre-of-momentum frame. Since the final state consists of spin-1/2 particles, the $\bar{\mathrm{p}}\mathrm{p} \to \bar{\Lambda}\Lambda$ T matrices will also be 4×4. All of the physics of the transition is contained in the $T(\theta)$ matrices, and it is here that models of the underlying process can be used to make predictions to compare with experimental

results. In general, after the transition indicated by Eq. (2), the resulting density matrix will no longer be separable.

As usual in the density matrix formalism, the observables of the experiment are calculated by taking the trace of the product of the density matrix and the matrix representing the operator of interest. For example, in the $\bar{\mathrm{p}}\mathrm{p} \to \bar{\Lambda}\Lambda$ case we have for the differential cross-section $\mathrm{d}\sigma/\mathrm{d}\Omega = (\mathrm{tr}\,\rho_{\bar{\Lambda}\Lambda}/\mathrm{tr}\,\rho_{\bar{\mathrm{p}}\mathrm{p}})$ and for the spin observables

$$P_{\bar{y}} = \frac{\mathrm{tr}\,(\rho_{\bar{\Lambda}\Lambda} \cdot \sigma_{\bar{y}} \otimes I_{\Lambda})}{\mathrm{tr}\,\rho_{\bar{\Lambda}\Lambda}}\ , \tag{3}$$

$$C_{\bar{m}n} = \frac{\mathrm{tr}\,(\rho_{\bar{\Lambda}\Lambda} \cdot \sigma_{\bar{m}} \otimes \sigma_{n})}{\mathrm{tr}\,\rho_{\bar{\Lambda}\Lambda}}\ ,\ \text{etc.} \tag{4}$$

Here $\hat{y}$ is the direction perpendicular to the reaction plane: $\hat{y} = \vec{p}_{\bar{\mathrm{p}}} \times \vec{p}_{\bar{\Lambda}}/|\vec{p}_{\bar{\mathrm{p}}} \times \vec{p}_{\bar{\Lambda}}|$, and the $\bar{\Lambda}$ polarization in the $\hat{y}$ direction is denoted by the notation $P_{\bar{y}}$.

The final-state $\bar{\Lambda}\Lambda$ density matrix $\rho_{\bar{\Lambda}\Lambda}$ can be expressed in terms of any complete set of 4×4 matrices. Fortunately, in the spin-1/2 on spin-1/2 case, this set can be chosen [35] to be those matrices corresponding to the usually observed experimental quantities of interest, namely

$$\begin{aligned}\rho_{\bar{\Lambda}\Lambda} = \ & \tfrac{1}{4} \cdot \mathcal{I}(\theta_{\bar{\Lambda}})\,[\, I_{\bar{\Lambda}} \otimes I_{\Lambda} + \vec{\sigma} \cdot \vec{P}_{\bar{\Lambda}} \otimes I_{\Lambda} \\ & + I_{\bar{\Lambda}} \otimes \vec{\sigma} \cdot \vec{P}_{\Lambda} + \sum_{\bar{m}n} C_{\bar{m}n}\, \sigma_{\bar{m}} \otimes \sigma_{n}\,]\ .\end{aligned} \tag{5}$$

Here the $C_{\bar{m}n}$ are the spin correlation coefficients of the $\bar{\Lambda}\Lambda$ pair, with the $(\bar{m}, n)$ indices denoting the axes of the $\bar{\Lambda}\Lambda$ rest mass coordinate system as defined in Fig. 2. The quantity $\mathcal{I}(\theta)$ is proportional to the differential cross-section.

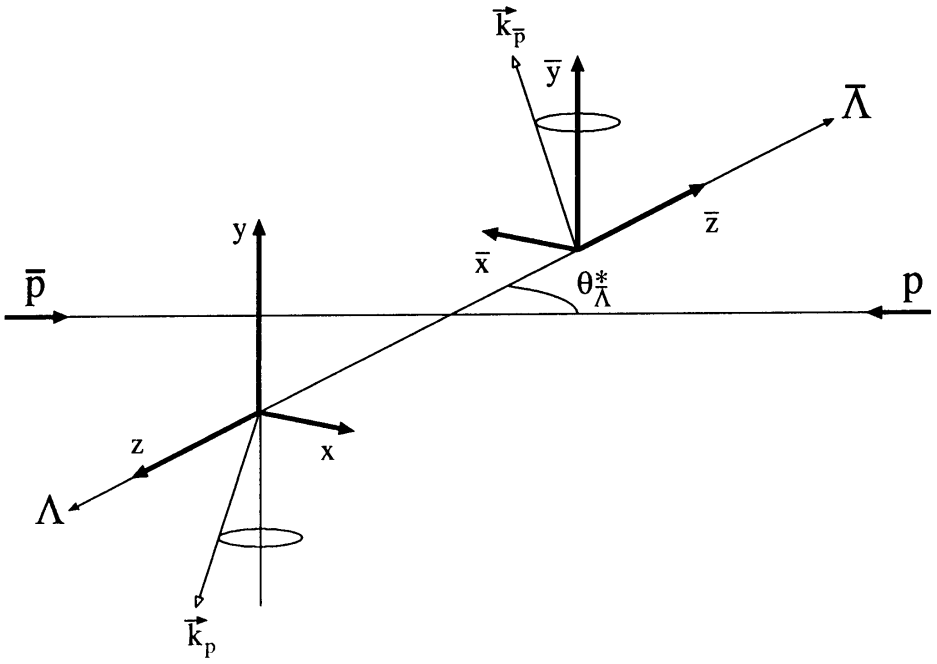

Figure 2: Definition of the coordinates in the $\bar{\mathrm{p}}\mathrm{p}$ and $\bar{\Lambda}\Lambda$ centre-of-momentum system and in the $\bar{\Lambda}$ and Λ rest frames.

Due to the self-analysing weak decay of the Λ hyperon [62] and the high intensity of the LEAR beam, all of these quantities are experimentally observable in PS185 in a statistically significant sample and therefore the spin orientations in the exit hyperon channel are known. The angular distribution of the weak-decay products can be obtained by calculating the density matrix for the final state [35] using the T-matrices for the weak decays:

$$\rho_{\bar{\mathrm{p}}\pi^+;\,\mathrm{p}\pi^-} = T_w\,\rho_{\bar{\Lambda}\Lambda}\,T_w^\dagger \ . \tag{6}$$

Since each Λ and $\bar{\Lambda}$ decay is independent, T_w is an outer product of 2×2 matrices, one for each particle [35].

The two present-day dynamical approaches — the s-channel quark–gluon model and the t-channel K-exchange process — are equally successful at describing the experiments. There seems to be little in the present data to distinguish between them, especially with respect to the cross-section information. However, the polarization and spin correlation measurements of the final-state $\bar{\Lambda}\Lambda$ hyperons are much more sensitive to model input, so we look to them for ways to distinguish between calculations. As outlined above, these quantities are quantum-mechanical expectation values of operators constructed from the Pauli matrices, for example,

$$\vec{P}_{\bar{\Lambda}} = \langle \vec{\sigma}_{\bar{\Lambda}} \otimes I_\Lambda \rangle \quad \text{and} \quad C_{\bar{m}n} = \langle \sigma_{\bar{m}} \otimes \sigma_n \rangle \, . \tag{7}$$

The number of independent spin observables is reduced substantially because of parity (P) conservation and charge conjugation (C) symmetry. Parity requires that all components of polarization *induced by the strong interaction and lying in the reaction plane* must vanish. So, for an unpolarized initial state, we have $P_x = P_z = P_{\bar{x}} = P_{\bar{z}} = 0$. C-parity adds the requirement that $P_{\bar{y}} = P_y$. P and C also impose strong restrictions on the correlation coefficients: $C_{\bar{x}y} = C_{\bar{y}x} = C_{\bar{z}y} = C_{\bar{y}z} = 0$ due to P, and $C_{\bar{z}x} = C_{\bar{x}z}$ due to C. However, if instead we begin with a polarized target, as we plan to do in forthcoming measurements of the depolarization [65], these statements will be modified.

The final-state angular distribution can be written out in full using Eqs. (5) and (6), giving

$$\begin{aligned} W(\cos\theta_{\bar{\Lambda}}; \hat{k}_{\bar{p}}, \hat{k}_p) \ &= \ \frac{1}{16\pi^2}[1 + \alpha P_y \cos\,\theta_y + \bar{\alpha} P_{\bar{y}} \cos\,\theta_{\bar{y}} \\ &\quad + \alpha\bar{\alpha} \sum_{\bar{m}n} C_{\bar{m}n} \cos\,\theta_{\bar{m}} \cos\,\theta_n] \ , \end{aligned} \tag{8}$$

where $\hat{k}_{\bar{p}}$ and $\hat{k}_p$ are the direction cosines of the outgoing products of the hyperon decays defined in the hyperon rest frame (see Fig. 2). CP invariance requires that $\alpha = -\bar{\alpha}$. The reported value of α is 0.642 ± 0.013 [63].

Using the angular distribution given in Eq. (8), and taking the angular acceptance into account, the polarizations and the spin correlation coefficients obtained by observing N events (i.e. the expectation values) can be expressed in terms of measured values of the direction cosines [35]. For the polarization, averaging Eq. (8) over N measurements yields

$$P_{\bar{y}} = \frac{3}{\bar{\alpha}} \cdot \frac{1}{N} \times \frac{\sum_{k=1}^{N} \ \zeta_k \cdot \cos\theta_{\bar{y}}^k}{\sum_{k=1}^{N} \zeta_k} \ , \tag{9}$$

while for the correlation coefficient we obtain

$$C_{\bar{m}n} = \frac{9}{\bar{\alpha}\alpha} \times \frac{\sum_{k=1}^{N} \ \zeta_k \cdot \cos\theta_{\bar{m}}^k \cdot \cos\theta_n^k}{\sum_k \zeta_k} \ . \tag{10}$$

Here ζ_k is the correction factor for the detector acceptance for each event k. For sufficiently large statistics N the standard deviation in $C_{\bar{m}n}$ is $\sigma_{\bar{m}n} \approx 3/(\alpha^2\sqrt{N})$.

Special attention was paid to understanding and correcting for systematic experimental uncertainties [20]. For this reason 350 000 Monte Carlo events were generated using isotropic distributions for the reaction products in the centre-of-momentum frame and in the rest frames of the $\bar{\Lambda}$ and Λ. This is tantamount to assuming unpolarized hyperon decays. The Monte Carlo sample was analysed by taking the full detector response into account using the same analysis program as for the real data. It was found that the spatial distributions of the decay antiprotons show a loss of events (see Fig. 3) in the region where the acceptance is small ($-1.0 \leq \cos\theta_{\bar{\Lambda}} \leq -0.33$). An equivalent situation occurs for the Λ decay, where an acceptance close to zero is observed for large centre-of-mass angles. These losses are explained by the low momenta of the π mesons from the Λ decays, which were not recorded in the detector system and/or were rejected by the requirements of the analysis program. When the acceptance factor ζ is zero in Eqs. (9) and (10), the correction is undefined.

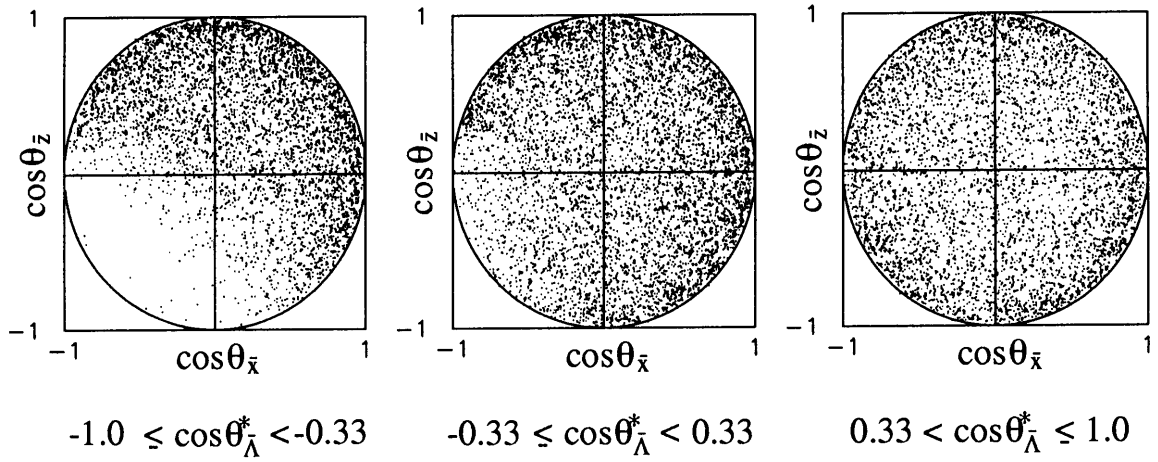

Figure 3: Projection of the unit vector end-point onto the $\bar{\Lambda}\Lambda$ production plane for the decay $\bar{\mathrm{p}}$ in the $\bar{\Lambda}$ rest frame. The ranges for the cosine of the scattering angle, from left to right, are -1.0 to -0.33, -0.33 to 0.33, and 0.33 to 1.0. Fainter regions correspond to inefficiencies.

In order to overcome these deficiencies, symmetry relations from the CPT theorem were used to generate three additional combinations of kinematic variables that give rise to the same result for the polarization and spin correlation observables. For an arbitrary set of vectors $\hat{k}_{\bar{p}}$ and $\hat{k}_p$:

- CP invariance allows the interchange of Λ and $\bar{\Lambda}$ (a symmetry with respect to the reaction plane);
- C and P invariance provide a reflection symmetry about the $\bar{y}$ and y axes;
- T invariance allows the exchange $\hat{r} \rightarrow -\hat{r}$.

If the measured pattern is replaced, event-by-event, by any one of the equivalent transformed patterns, the resulting polarization observables will be unchanged. Therefore the event sample can be 'extended' to a sample which is four times larger, and more importantly, one which allows each event to effectively contribute in four ways to the

angular distributions. While this greatly improves our understanding of the systematics of the experiment, it *does not* of course improve the statistical accuracy.

If the acceptance function is uniform, these four events contribute with equal weight to the determination of the spin correlation coefficients. Thus, a smooth acceptance function can be constructed which is everywhere greater than zero, and which consequently provides sufficient information to determine the differential spin-correlation coefficients $C_{\bar{x}x}$, $C_{\bar{y}y}$, $C_{\bar{z}z}$, and $C_{\bar{x}z} = C_{\bar{z}x}$ in the entire centre-of-momentum space.

In an additional investigation, an *uncorrelated sample* of events was obtained from the data themselves. To do this, all analysed $\bar{\Lambda}_n\Lambda_n$ events were ordered according to their production kinematics and then recombined with nearest neighbours to make hypothetical events, e.g. $\bar{\Lambda}_n\Lambda_{n+1}$. This gave an event sample which was by construction uncorrelated, allowing the experimental acceptance function ζ to be measured directly. The two methods — the Monte Carlo simulation and the recombination procedure — agree rather well [20]. Differences are of the order of 10% and largest in the very forward and backward regions. They indicate where there are poorly understood detector efficiencies.

5 Results

5.1 Cross-sections

For the 1.642 GeV/c data, approximately 7.2×10^{10} antiprotons were incident on the target, giving an integrated luminosity of $\mathcal{L} = 5.1$ nb^{-1}, whereas at 1.918 GeV/c, approximately 5.4×10^{10} incident antiprotons produced a luminosity of $\mathcal{L} = 3.2$ nb^{-1}. At the lower momentum, 43 430 reconstructed events gave a total cross section of $\sigma_{\rm tot} = 64.1 \pm 0.4 \pm 1.6$ μb, while for the higher momentum 36 977 events led to $\sigma_{\rm tot} = 88.0 \pm 0.7 \pm 1.9$ μb. The first and second error quoted are statistical and systematic, respectively. The differential cross-sections and polarizations are shown in Figs. 4(a) and 4(c) as a function of centre-of-momentum $\cos\theta_{\bar{\Lambda}}$, and in Figs. 4(b) and 4(d) as a function of the reduced four-momentum transfer squared, t':

$$t' \;=\; -t(\theta = 0) + m_{\rm p}^2 + m_{\Lambda}^2 - \frac{s}{2} + \frac{1}{2}\sqrt{(s - 4m_{\rm p}^2)(s - 4m_{\Lambda}^2)}\;\cos\theta_{\bar{\Lambda}}. \qquad (11)$$

The differential cross-sections on a logarithmic scale, shown in Fig. 4(a), reveal in general the typical behaviour for the $\bar{\rm p}{\rm p} \to \bar{\Lambda}\Lambda$ reaction, as already observed at lower momenta: a sharp forward rise is followed by a rather flat distribution. Such a forward-peaked angular distribution is typical for peripheral processes and for simple absorptive models [32]–[33]. The slope parameter of 9.1 ± 0.5 (GeV/c)$^{-2}$, as extracted from Fig. 4(b), corresponds to an absorption radius of 1.2 $\pm$ 0.1 fm. Similar values were deduced for the measurements in the threshold region [66]–[68].

At lower incident momenta the slope change from steeply rising to flat for angular distributions occurs at $t' \simeq -0.2$ (GeV/c)^2. For the high momenta discussed here — especially for the 1.918 GeV/c data — this slope change occurs at a more negative value of t', as can be seen in Fig. 4b. For the 1.642 GeV/c data, the slope change is smooth with an indication of a break at $t' = -0.2$ (GeV/c)^2, and a clear turnover to a flat distribution shifted to a value of $t' \simeq -0.35$ (GeV/c)^2. For the 1.918 GeV/c data, significant flattening is not observed until $t' \simeq -0.60$ (GeV/c)^2, again with a smooth change of the slope towards the steep rise at small scattering angles. In this model a comparison of the two measured cross sections implies that there is a larger absorption radius for the 1.918 GeV/c data.

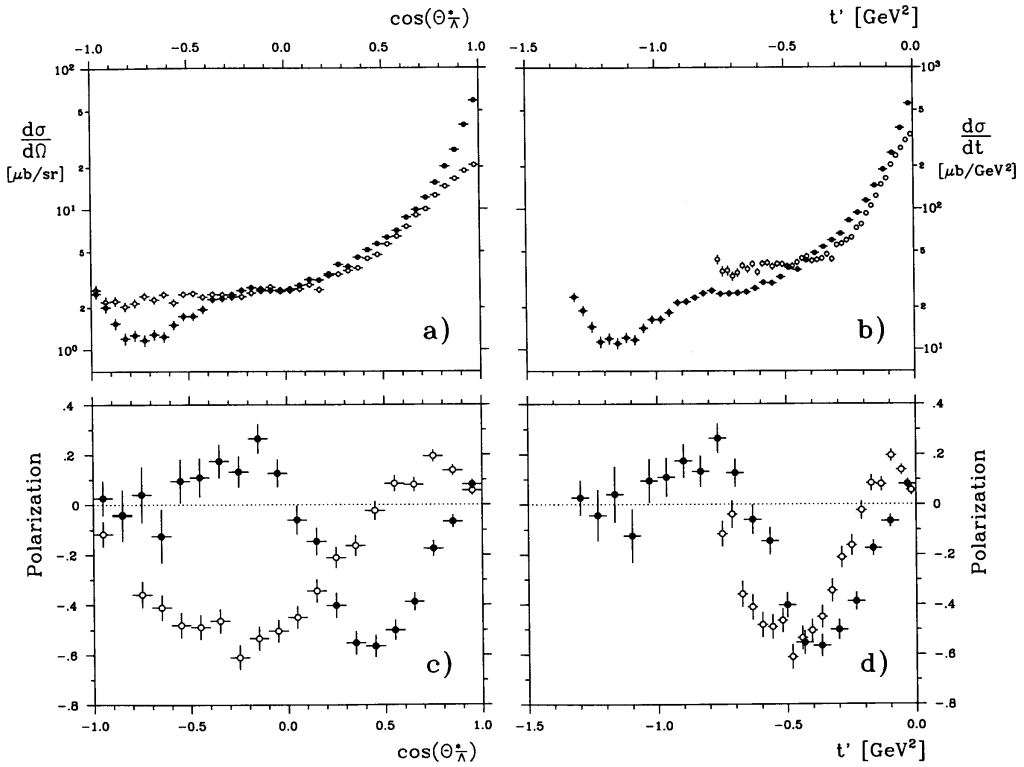

Figure 4: Cross-sections (upper graphs) and polarizations (lower graphs) from this experiment. Open and closed circles represent data obtained at 1.642 and 1.918 GeV/c, respectively. The left-hand graphs (a) and (c) show the data as a function of $\cos\theta$. The right-hand graphs (b) and (d) show the data as function of reduced four-momentum transfer squared, t'.

It is interesting to note the apparent dip in the differential cross-section at back angles, especially for the higher momentum data at 1.918 GeV/c. If real, this observation could indicate new reaction mechanisms and/or nucleon structures. For example, in a meson- or baryon-exchange picture, such features have been interpreted in terms of u-channel baryon exchanges [69]. In quark descriptions, such oscillations can be obtained from models in which spatially-extended 'di-quarks' [47] are taken to be elementary constituents of baryons in addition to the point-like quarks of the constituent scattering model. However, a word of caution is necessary since the backward increase could be due very simply to a wrong baryon number identification between $\bar{\Lambda}$ and Λ. A permutation in 4% of the cases could produce the backward increase that is observed. Although we are confident of our analysis, we do not wish to place strong emphasis on the physics interpretation given the small margin for error.

With regard to the reaction dynamics, it is obvious that at higher beam momenta contributions from higher partial waves will be observed. This is seen in the slope of the differential cross-section as well as by comparing the Legendre polynomial coefficients, extracted to fit the experimental data (Table 1). It should be noted that the appearance of the coefficient A_8 is closely linked to the back-angle structure discussed in the above paragraph.

Table 1: Coefficients resulting from Legendre Polynomial fits to the $\bar{p}p \rightarrow \bar{\Lambda}\Lambda$ differential cross-sections obtained at 1.642 and 1.918 GeV/c

Coefficient	Value $\pm$ Error 1.642 GeV/c	Value $\pm$ Error 1.918 GeV/c
A_0	5.097 $\pm$ 0.035	7.033 $\pm$ 0.053
A_1/A_0	1.238 $\pm$ 0.018	1.775 $\pm$ 0.023
A_2/A_0	1.195 $\pm$ 0.022	1.919 $\pm$ 0.031
A_3/A_0	0.738 $\pm$ 0.024	1.659 $\pm$ 0.035
A_4/A_0	0.028 $\pm$ 0.027	1.374 $\pm$ 0.037
A_5/A_0	-0.041 ± 0.029	0.826 $\pm$ 0.036
A_6/A_0	-0.065 ± 0.031	0.622 $\pm$ 0.035
A_7/A_0	-0.094 ± 0.029	0.337 $\pm$ 0.029
A_8/A_0	-0.009 ± 0.028	0.118 $\pm$ 0.023

5.2 Polarization

Because the antihyperon–hyperon pair is produced in a strong interaction process, parity conservation allows only the polarization component perpendicular to the reaction plane (i.e. the $\hat{y}$ direction) to be non-zero (assuming an unpolarized initial state). In addition, since the reaction plane is undefined at $\theta_{\bar{\Lambda}} = 0$ and π, the polarization must vanish there. In Fig. 4 the polarizations averaged over $\bar{\Lambda}$ and Λ are shown both as a function of $\cos\theta_{\bar{\Lambda}}$ (Fig. 4c) and as a function of the reduced square of the momentum transfer t' (Fig. 4d). The open and closed circles are the data obtained at 1.642 and 1.918 GeV/c, respectively. The 1.642 GeV/c data exhibit polarization characteristics similar to those observed previously at lower beam momenta [21]–[23]: $P_{\bar{y}} > 0$ over the range $t' = 0$ to $t' = -0.2$ (GeV/c)^2; it crosses zero at that point and remains negative with decreasing t' until the minimum value of t' is reached. The 1.918 GeV/c data illustrate somewhat different behaviour in that the initial sign change occurs at a much lower value of t' [-0.08 (GeV/c)^2] [20]. In addition, while at 1.642 GeV/c only one zero crossing is observed, the 1.918 GeV/c data show a second one at 90° centre-of-momentum angle, or $t' = -0.65$ (GeV/c)^2. This value is rather close to the point at which the shape change of the differential cross-section occurs. At larger reduced squared momentum transfers, $|t'| > 1.1$ (GeV/c)^2 (equivalent to $-0.7 < \cos\theta_{\bar{\Lambda}} < -1.0$) the polarization is consistent with zero.

5.3 Spin correlations and singlet fractions

In Fig. 5a the differential spin correlation coefficient distributions are shown. The errors are dominated by statistics and thus increase at large angles where the differential cross-section is small. As for the case of the polarization, the reaction plane is undefined at $\cos\theta_{\bar{\Lambda}} = \pm 1$, so it is expected that $C_{\bar{x}z} = C_{\bar{z}x} = 0$ and that $C_{\bar{x}x} = -C_{\bar{y}y}$ at these angles. The data in Fig. 5a are consistent with these statements.

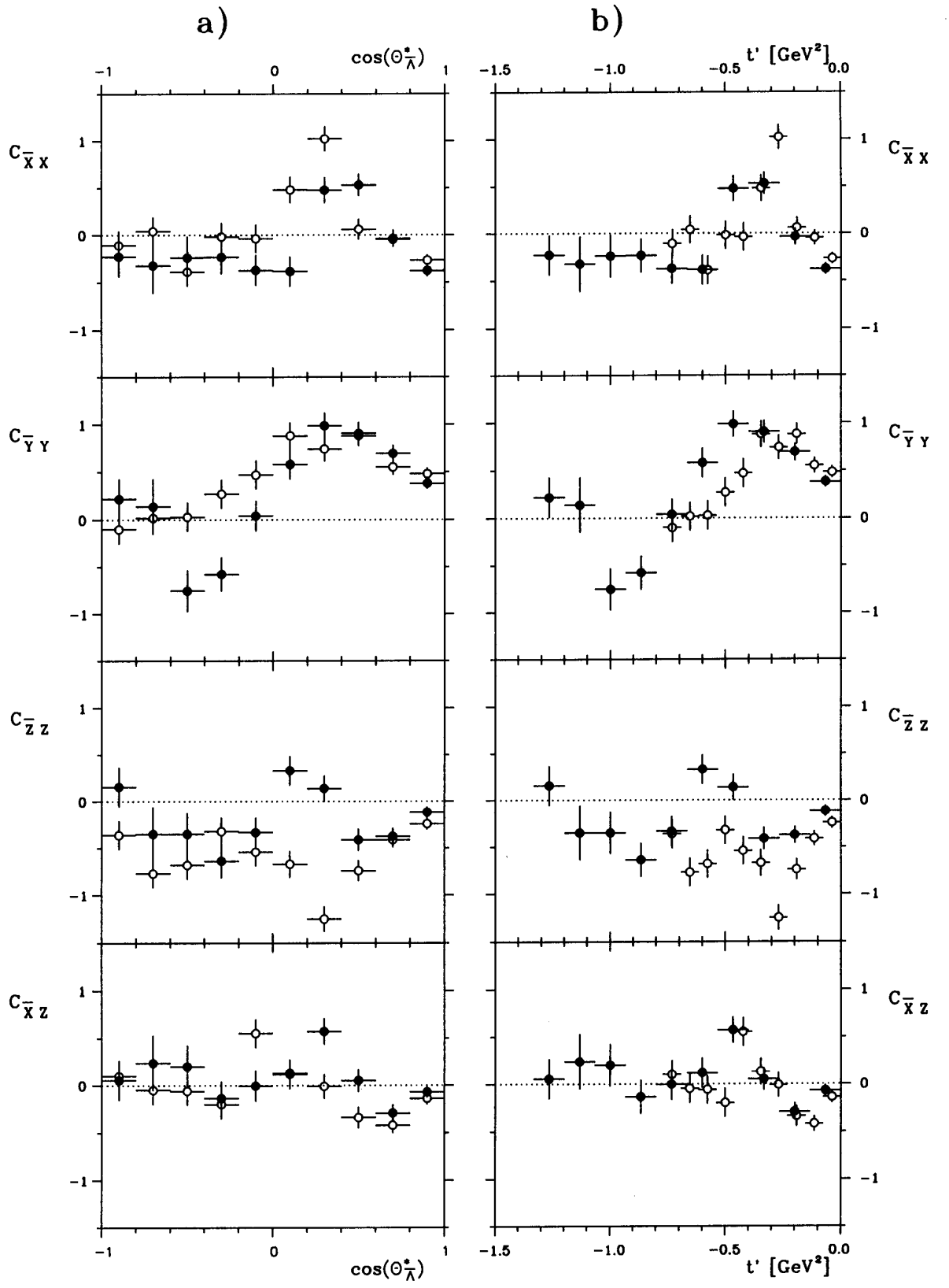

Figure 5: Spin correlations. Open and closed circles represent data obtained at 1.642 and 1.918 GeV/c, respectively. Graph (a) shows the data as a function of $\cos\theta$. Graph (b) shows the data as a function of reduced four-momentum transfer squared, t'.

The coefficient $C_{\bar{y}y}$ is positive for angles of $\theta_{\bar{\Lambda}} \leq 90°$, with a maximum value close to unity at $\cos\theta_{\bar{\Lambda}} \simeq 0.3$. While the 1.918 GeV/$c$ data show negative spin-correlation values for scattering angles of $\theta_{\bar{\Lambda}} \leq 90°$, the values for the 1.642 GeV/c spin correlations decrease to around zero. Less pronounced structures are observed for the other correlation coefficients. Figure 5b shows the spin correlations as a function of the reduced momentum transfer t'.

The three diagonal elements of the spin-correlation matrix are combined to form the singlet fraction S_F

$$S_F = \frac{1}{4}(1 - \langle\vec{\sigma}_{\bar{\Lambda}} \cdot \vec{\sigma}_{\Lambda}\rangle) = \frac{1}{4}(1 + C_{\bar{x}x} - C_{\bar{y}y} + C_{\bar{z}z}) \ , \tag{12}$$

where the coordinate system is the one given in Fig. 2. The expected value for S_F when there is no spin correlation is 1/4, determined by simple statistical weighting of the three triplet and one singlet magnetic states.

The differential singlet fraction is shown in Fig. 6. Averaging over all angles yields $\langle S_F\rangle = -0.003 \pm 0.015$ for the 1.642 GeV/c data, and $\langle S_F\rangle = 0.058 \pm 0.016$ for the 1.918 GeV/c data.

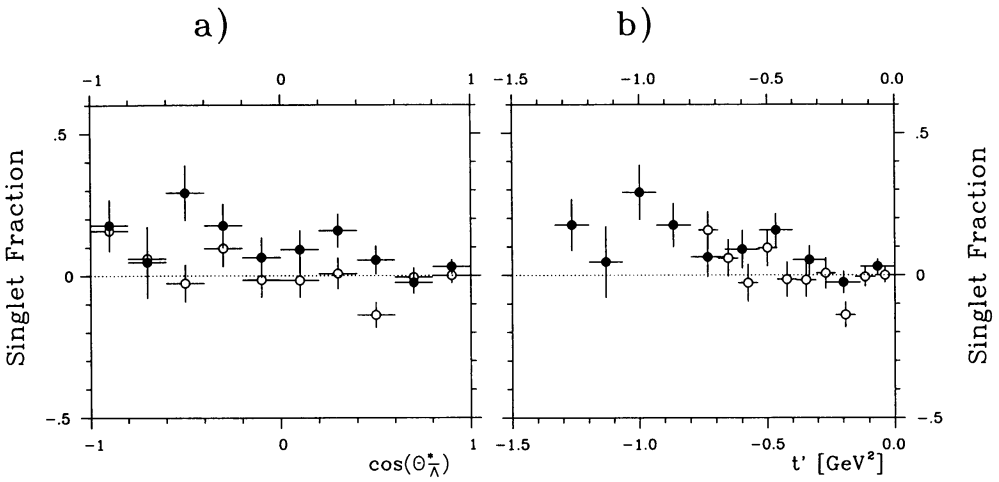

Figure 6: Singlet fractions. Open and closed circles represent data obtained at 1.642 and 1.918 GeV/c, respectively. Graph (a) shows the data as a function of $\cos\theta$. Graph (b) shows the data as a function of reduced four-momentum transfer squared, t'. The unweighted statistical value would be 1/4.

The data at the lower momentum give $\langle S_F\rangle$ values which are consistent with zero, indicating a pure triplet production of the $\bar{s}s$ strange-quark pair. The 1.918 GeV/c data give a slightly positive value with a $3.5\,\sigma$ confidence interval. This measurement is the first with high statistics above the $\bar{p}p \rightarrow \bar{\Sigma}^0\Sigma^0$ thresholds and could reflect a coupling to these channels.

It will be interesting to see whether the observed non-zero value for $\langle S_F\rangle$ at 1.918 GeV/c is confirmed by additional measurements taken by the PS185 Collaboration around the $\bar{\Sigma}^0\Sigma^0$ and $\bar{\Sigma}^{\pm}\Sigma^{\mp}$ thresholds. As the absolute value of the momentum transfer increases, the trend of the data seems to be away from pure triplet production, and possibly toward the statistically expected mixture.

5.4 A test for CP violation

CP violation has only been observed in neutral-kaon systems. Though several models can account for CP violation [70]–[74], the effects seen in the current weak-interaction data are still not adequate for distinguishing between these models. As described in [26] we evaluate the asymmetry parameter A, defined as

$$A = \frac{\alpha + \bar{\alpha}}{\alpha - \bar{\alpha}} \ , \tag{13}$$

using the present data. Here α and $\bar{\alpha}$ are the decay parameters for the non-leptonic Λ and $\bar{\Lambda}$ weak decays. A non-zero value of A would indicate a direct CP violation. Owing to the weak decay $\bar{\Lambda} \rightarrow \bar{p}\pi^+$ the angular distribution of the $\bar{\mathrm{p}}$ from the $\bar{\Lambda}$ decay is

$$I(\theta_{\bar{\mathrm{p}}}) = I_0 \left(1 + \bar{\alpha} P_{\bar{y}} \cdot \cos\theta_{\bar{\mathrm{p}}}\right) \ , \tag{14}$$

with $\theta_{\bar{\mathrm{p}}}$ being defined in the $\bar{\Lambda}$ rest frame between the decay $\bar{\mathrm{p}}$ direction and the $\bar{y}$ axis (see Fig. 2). Adapting the 'method of weighted sums' [75] for a sample of N decaying $\bar{\Lambda}$ particles leads to the expression

$$\bar{\alpha} P_{\bar{y}} = \frac{\sum_{k=1}^{N} \cos\theta_{\bar{\mathrm{p}}}^{k}}{\sum_{k=1}^{N} \cos^2\theta_{\bar{\mathrm{p}}}^{k}} \ . \tag{15}$$

Invariance of the strong force under C parity requires $P_{\bar{y}}(\cos\theta) = P_y(\cos\theta)$, allowing A to be determined from the experimental data using Eq. (13).

In Fig. 7 the differential values of A are presented for both momenta, the upper data from 1.642 GeV/c, and the lower from 1.918 GeV/c. Large error bars (or missing values) arise due to small values of the respective polarizations (see Fig. 4). The data are consistent with zero at both incident $\bar{\mathrm{p}}$ momenta. Our evaluation yields mean values of

$$\begin{aligned} \langle A\,(1.642\,GeV/c)\rangle &= 0.026 \pm 0.030 \quad \text{and} \\ \langle A\,(1.918\,GeV/c)\rangle &= 0.010 \pm 0.037 \ . \end{aligned} \tag{16}$$

Combining the present results with earlier published measurements of the PS185 experiment (totalling 95 832 events) leads to an asymmetry parameter of $\langle A \rangle = 0.013 \pm 0.022$. While this result represents the best measurement to date of CP violation outside the neutral-kaon system, it is still at least an order of magnitude away from providing a test of theoretical models. However, there still remains a considerably larger set of PS185 data which have not been included here, and which, when analysed, will reduce the error on the CP-violation limit further.

5.5 A test of the CPT theorem

According to quantum field theory, the CPT invariance theorem applies very generally to particle interactions. CPT invariance requires equal rest masses and lifetimes for a particle and its antiparticle. The decay length of the hyperons is proportional to the product of momentum and lifetime τ. The lifetime distribution follows a simple exponential law:

$$\frac{\mathrm{d}N}{\mathrm{d}t} = N_0 \cdot \mathrm{e}^{-t/\tau} \ . \tag{17}$$

Thus, with the present experimental set-up the lifetime distributions of both $\bar{\Lambda}$ and Λ could be extracted for a given momentum in the same experiment. Figure 8 shows the results for the 1.642 GeV/c data [4]. The lifetime values extracted are

$$\tau_{\bar{\Lambda}} = 258.4 \pm 4.7 \pm 5.3 \text{ ps} ,$$
$$\tau_{\Lambda} = 265.2 \pm 4.3 \pm 5.3 \text{ ps} . \quad (18)$$

The first and second uncertainties given are statistical systematic, respectively. Using extensive Monte Carlo simulations these results have been corrected for the specific features of our detector.

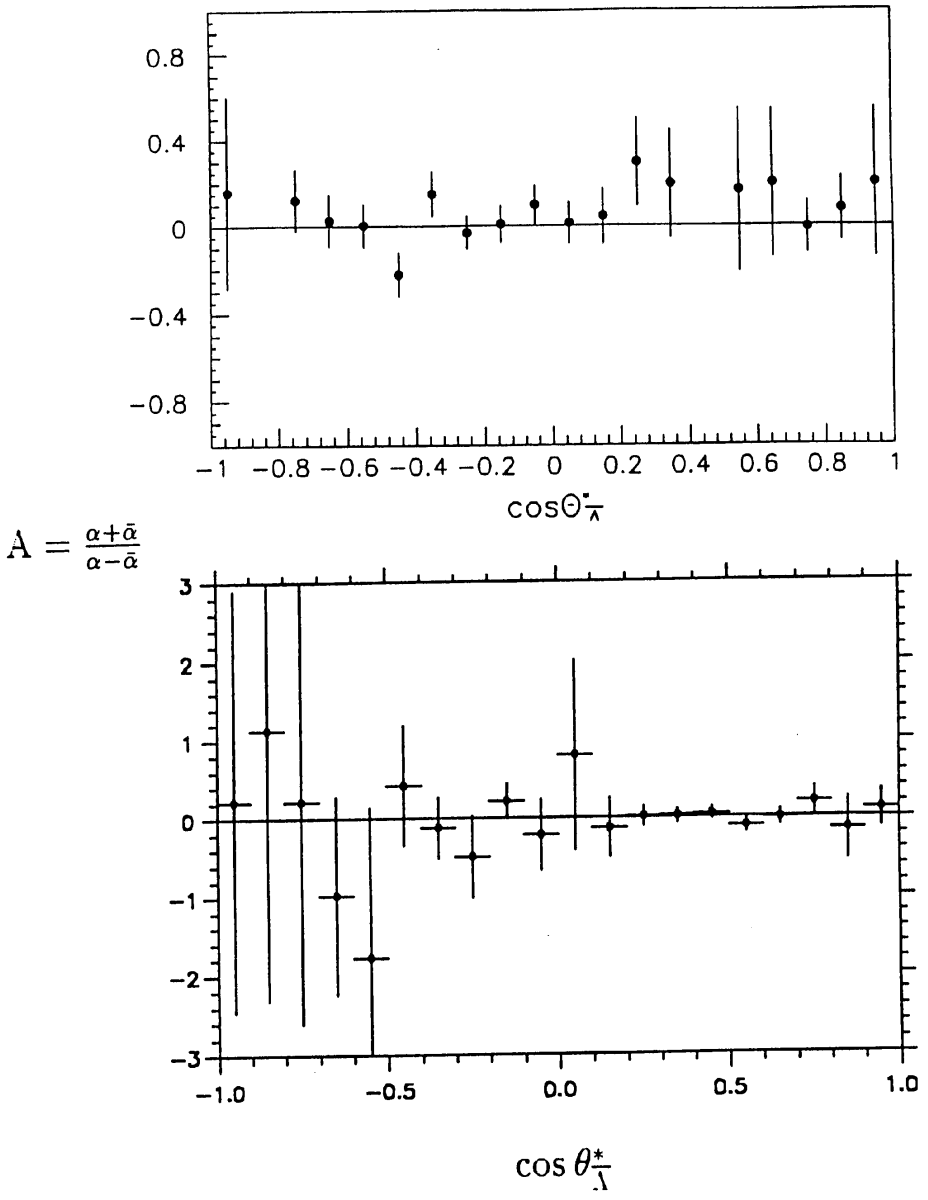

Figure 7: Angular distributions of the ratio $A = \langle(\alpha+\bar{\alpha})\rangle / \langle(\alpha-\bar{\alpha})\rangle$. The top and bottom graphs show data obtained at 1.642 and 1.918 GeV/c, respectively.

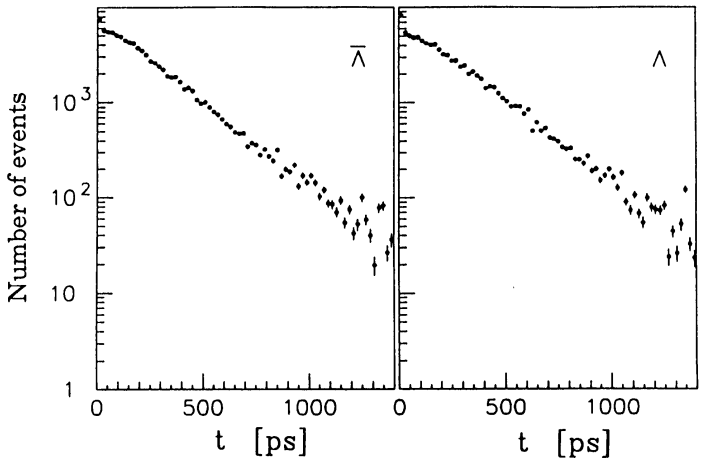

Figure 8: Lifetime distributions of $\bar{\Lambda}$ (left) and Λ (right), corrected using Monte Carlo simulations.

In order to reduce the Monte Carlo corrections on the lifetime measurements when comparing the $\bar{\Lambda}$ and Λ lifetimes, momentum and decay-point dependent cuts were applied. Thus, the detector acceptance was assumed to be equal in certain regions for the hyperon decay products. This special sampling led to a ratio of

$$R = \frac{\tau - \bar{\tau}}{\frac{\tau+\bar{\tau}}{2}} = (-1.8 \pm 6.6 \pm 5.6) \times 10^{-3}. \tag{19}$$

Details are presented elsewhere. This evaluation is an order-of-magnitude more precise than the only other measurement [76] reported to date.

6 Discussion

Differential cross-sections, polarizations, and spin correlations have been presented at incident antiproton momenta of 1.642 and 1.918 GeV/c for the reaction $\bar{p}p \to \bar{\Lambda}\Lambda \to \bar{p}\pi^+ p\pi^-$. There are about 40 000 reconstructed events in each sample.

The angular distributions shown in Fig. 4 indicate that the slope of the data at small angles is significantly steeper for the 1.918 GeV/c data than for the 1.642 GeV/c data. This would seem to indicate a larger interaction range at the higher momentum. In both cases, as in all previous measurements performed by PS185, the forward peaking dissolves at larger angles into an almost flat, featureless distribution.

The differential polarizations at the two momenta exhibit structures that are distinct from each other, the higher momentum data displaying an additional node. As suggested from the differential cross-sections, higher partial wave contributions and their coherent interference are probably responsible for the change in the pattern from that observed at lower beam momenta. The influence of a coupled-channel effect on the structure should be further investigated in high statistics measurements below and above the $\bar{p}p \to \bar{\Sigma}^{\pm}\Sigma^{\pm}$ channels.

The weighted mean of all the measured singlet-fraction data from the PS185 experiment published to date, $\langle S_F \rangle = 0.007 \pm 0.009$, is consistent with zero. This indicates that $\Lambda\bar{\Lambda}$ production is occurring in a pure triplet state. However, at 1.918 GeV/c a small but positive value of $\langle S_F \rangle = 0.058 \pm 0.016$ was observed, which may indicate that at

higher absolute values of the momentum transfer, $\Lambda\bar{\Lambda}$ production tends toward the value expected from simple spin statistics.

In the naïve quark model the lowest-order process for the $\bar{p}p \to \bar{\Lambda}\Lambda$ reaction is the annihilation of a $\bar{u}u$ quark pair followed by the production of an $\bar{s}s$ quark pair. In these models the other quark pairs in the participating baryons are regarded as spin and isospin $S = I = 0$ spectators that do not influence the reaction dynamics. Most of the quark model applications calculate the s-channel vector ($^3S_1$) and/or scalar ($^3P_0$) exchange only, and necessarily result in $S_F = 0$ triplet $\bar{s}s$ pair production. Following [43] a pseudoscalar s-channel exchange could proceed via the exchange of an intermediate η or η', since these mesons possess strong strange–antistrange quark-flavour content. In this case, the pseudoscalar contribution is weak due to small coupling constants and high spin multiplicities. Qualitatively, the present small value of $\langle S_F \rangle$ is in agreement with these considerations.

In a t-channel meson-exchange picture [35], [37], [38] interferences between the K, K^*, and K^{**} meson exchanges are needed in order to enhance the strong tensor component and to partially cancel the central potential components. Calculations result in a singlet fraction $\langle S_F \rangle$ of only a few percent, whereas a decrease of K–K^* interference would lead to an increased S_F contribution. According to [60] a large tensor transition ($\ell - \ell' = 2$) in $\bar{p}p \to \bar{\Lambda}\Lambda$ is expected due to the strong tensor force of the K–K^* exchange. This is one reason why the PS185 Collaboration will measure the depolarization in the $\bar{p}p \to \bar{\Lambda}\Lambda$ reaction employing a frozen-spin target [77].

As expected with the present accuracy, CP violation effects in the weak interaction were not observed in either experiment presented here. Combining the present results with earlier published measurements of PS185 (totalling 95 832 events) leads to an asymmetry parameter of $\langle A \rangle = 0.013 \pm 0.022$. This value is essentially consistent with zero. However, the PS185 experiment is still a few orders of magnitude away from providing enough statistics to test present theoretical models. Similarly, for the CPT test, the lifetimes of both $\bar{\Lambda}$ and Λ were found to be identical at the 10^{-3} level.

In the near future, the PS185 collaboration would like to publish data for their $\Lambda\bar{\Lambda}$ channel at several other incident momenta and for other hyperon reaction channels. We expect that these data will extend our general understanding of this interesting set of reactions.

7 Acknowledgements

The members of the PS185 Collaboration would like to thank the LEAR accelerator team for their excellent preparation of the antiproton beam. We would also like to thank Professor Mary Alberg for a very helpful critique of our manuscript. We also gratefully acknowledge financial and material support from the Austrian Science Foundation, the German Bundesministerium für Forschung und Technologie, the Swedish Natural Science Research Council, the United States Department of Energy (contract DE-FG02-87ER 40315), and the United States National Science Foundation.

This work is based on the dissertations of H. Fischer and M. Ziolkowski, submitted to the Universities of Freiburg and Cracow, respectively, in partial fulfilment of the requirements for their Ph.D. degrees.

References

[1] R. Bröders, PhD thesis, KFA Jülich, Germany, 1995.

[2] H. Dennert, PhD thesis, Universität Erlangen–Nürnberg, Germany (in preparation).

[3] W. Dutty, PhD thesis, Universität Freiburg, Germany, 1988.
[4] H. Fischer, PhD thesis, Universität Freiburg, Germany, 1992.
[5] R. von Frankenberg, PhD thesis, Universität Erlangen–Nürnberg, Germany, 1989.
[6] R. Geyer, PhD thesis, Universität Erlangen–Nürnberg, Germany, 1993.
[7] J. Hauffe, PhD thesis, Universität Erlangen–Nürnberg, Germany (in preparation).
[8] T. Jones, PhD thesis, University of Illinois, Urbana–Champaign, USA (in preparation).
[9] R.–A. Kraft, PhD thesis, Universität Erlangen–Nürnberg, Germany, 1994.
[10] C. Maher, PhD thesis, Carnegie Mellon University, USA, 1986.
[11] S. Ohlssen, PhD thesis, University of Uppsala, Sweden, 1990.
[12] K. Sachs, PhD thesis, KFA Jülich, Germany, 1996.
[13] H. Schlederman, PhD thesis, Universität Freiburg, Germany, 1989.
[14] T. Sefzick, PhD thesis, KFA Jülich, Germany, 1991.
[15] G. Sehl, PhD thesis, KFA Jülich, Germany, 1989.
[16] J. Seydoux, PhD thesis, Carnegie Mellon University, USA, 1990.
[17] F. Stinzing, PhD thesis, Universität Erlangen–Nürnberg, Germany, 1991.
[18] R. Tayloe, PhD thesis, University of Illinois, Urbana–Champaign, USA, 1995.
[19] R. Todenhagen, PhD thesis, Universität Freiburg, Germany, 1995.
[20] M. Ziolkowski, PhD thesis, University of Cracow, Poland and KFA Jülich, Germany, 1993.
[21] P. Barnes et al., Phys. Lett. **B189** (1987) 249.
[22] P. Barnes et al., Phys. Lett. **B229** (1989) 432.
[23] P. Barnes et al., Nucl. Phys. **A526** (1991) 575.
[24] P. Barnes et al., Phys. Lett. **B331** (1994) 203.
[25] P. Barnes et al., Phys. Lett. **B246** (1990) 273.
[26] P.D. Barnes et al., Phys. Lett **B199** (1987) 147.
[27] B. Jayet et al., Nuovo Cimento **45A** (1978) 371.
[28] B.Y. Oh et al., Nucl. Phys. **B51** (1973) 57.
[29] S.M. Jacobs et al., Phys. Rev. **D17** (1978) 1187.
[30] H.W. Atherton et al., Nucl. Phys. **B69** (1974) 1.
[31] H. Becker et al., Nucl. Phys. **B141** (1978) 48.
[32] D. Perkins, *Introduction to High Energy Physics* (Addison-Wesley Publications, Reading, MA, 1987), Third Edition.
[33] M. Perl, *High Energy Hadron Physics* (John Wiley and Sons, New York, 1974).
[34] J. Niskanen, University of Helsinki preprint HU–TFT–85–28 (1985).
[35] F. Tabakin and R.A. Eisenstein, Phys. Rev. **C31** (1985) 1857.
[36] A. Green and J. Niskanen, Prog. Part. Nucl. Phys. **18** (1987) 93.
[37] M. Kohno and W. Weise, Phys. Lett. **B179** (1986) 15; Phys. Lett. **B206** (1988) 584; Nucl. Phys. **A479** (1988) 433c.
[38] W. Weise, Nucl. Phys. **A558** (1993) 219c.
[39] P. LaFrance and B. Loiseau, Nucl. Phys. **A528** (1991) 557;
P. LaFrance, B. Loiseau, and R. Vinh Mau, Phys. Lett. **B214** (1988) 317.
[40] Y. Lu and M. Locher, Z. Phys. **A346** (1993) 143.
[41] M. Alberg, E. Henley and L. Wilets, Z. Phys. **A331** (1988) 207.
[42] M. Alberg, E. Henley and L. Wilets, Phys. Rev. **C38** (1988) 1506.
[43] M. Alberg, E. Henley and W. Weise, Phys. Lett. **B255** (1991) 498.

[44] M. Alberg, E.M. Henley, L. Wilets and P.D. Kunz, Nucl. Phys. **A560** (1993) 365; and Proc. Second Biennial Workshop on Nucleon–Antinucleon Physics, Yu. Kalashnikova, L. Kondratyuk, A. Kudryavtsev and N. Smorodinskaya, Moscow, 1993 [Yadernaya Phyzika **57** (1994) 1678].
[45] H. Genz and S. Tatur, Phys. Rev. **D30** (1984) 63.
[46] G. Brix, H. Genz, and S. Tatur, Phys. Rev. **D39** (1989) 2054.
[47] P. Kroll, B. Quadder, and W. Schweiger, Nucl. Phys. **B316** (1989) 373.
[48] H. Genz, M. Nowakowski and D. Woitschitzky, Phys. Lett. **B260** (1991) 179.
[49] S. Furui and A. Faessler, Nucl. Phys. **A468** (1987) 669.
[50] M. Burkhardt and M. Dillig, Phys. Rev. **C37** (1988) 1362.
[51] J. Vandermeulen, Z. Phys. **C37** (1988) 563.
[52] H. Rubinstein and H. Snellman, Phys. Lett. **B165** (1985) 187.
[53] F. Tabakin, R.A. Eisenstein and Y. Lu, Phys. Rev. **C44** (1991) 1749.
[54] A. Kudriyavtsev and V. Samoilov, Mod. Phys. Lett. **A4** (1989) 721.
[55] A. Schneider-Neureither et al., Z. Physik **A344** (1993) 317.
[56] O. Dalkarov, K. Protasov and I. Shapiro, Int. J. Mod. Phys. **A5** (1990) 2155.
[57] I. Shapiro, Nucl. Phys. **A478** (1988) 665c.
[58] J. Carbonell, K. Protasov and O. Dalkarov, Nucl. Phys. **A558** (1993) 353c.
[59] R. Timmermans, T. Rijken and J. de Swart, Nucl. Phys. **A479** (1988) 383c; Phys. Rev. **D45** (1992) 2288; Phys. Lett. **B257** (1991) 227.
[60] J. Haidenbauer et al., Phys. Rev. **C45** (1992) 931; Phys. Rev. **C46** (1992) 2158 and 2516.
[61] Y. Lu and F. Tabakin, in preparation.
[62] L. Durand and J. Sandweiss, Phys. Rev. **135B** (1964) 540.
[63] Particle Data Group, Phys. Lett. **B239** (1990) 1.
[64] M. Jacob and G.C. Wick, Ann. Phys. **7** (1959) 404.
[65] B. Bassalleck et al., PS185 Collaboration, CERN–SPSLC/95–13 (1995).
[66] V. Barger and D. Cline, *Phenomenological Theories of High Energy Scattering* (W.A. Benjamin, Inc., New York, 1969).
[67] H. Schmitt et al., Proc. IXth European Symposium on Proton-Antiproton Interactions and Fundamental Symmetries, Mainz, Germany, 1988, eds. K. Kleinknecht and E. Klempt (Nucl. Phys. **B8**, 1989, 162).
[68] T. Johansson, Proc. Second Conference on Particle Production near Threshold, C. Ekstrom, B. Hoistad, A. Johansson and S. Kullander (Phys. Scr. Reprint Series No. 21, 1993, 102).
[69] R.A. Eisenstein, in Proc. Second Biennial Workshop on Nucleon–Antinucleon Physics, eds. Yu. Kalashnikova, L. Kondratyuk, A. Kudryavtsev and N. Smorodinskaya, Moscow, 1993 (Yadernaya Phyzika **58**, 1994, 1751).
[70] L. Wolfenstein, Phys. Rev. Lett. **13** (1964) 562.
[71] S. Weinberg, Phys. Rev. Lett. **37** (1976) 657.
[72] R.N. Mohapatra et al., Phys. Rev. **D11** (1975) 566.
[73] L.L. Chau, Phys. Rep. **95** (1983) 1.
[74] L. Wolfenstein, Annu. Rev. Nucl. Part. Sci. **36** (1986) 137.
[75] D. Besset et al., Nucl. Instrum. Methods **166** (1979) 515.
[76] J. Badier et al., Phys. Lett. **B25** (1967) 152.
[77] H. Dutz et al., Nucl. Instrum. Methods **A340** (1994) 272;
B. Bassalleck et al., Proposal P287, CERN/SPSLC 95–13 (accepted as PS185–3).